RSC Advances

ROYAL SOCIETY OF CHEMISTRY

www.rsc.org/advances

Preparation and characterization of poly(3-methylthiophene)/CeY zeolite composites

Pengyue Han, Junjie Liao, Jinyu Chang, Liping Chang, Weiren Bao*

(State Key Laboratory Breeding Base of Coal Science and Technology Co-founded by Shanxi Province and the Ministry of Science and Technology, Taiyuan University of Technology, Taiyuan 030024, PR China)

Abstract: Poly(3-methylthiophene)/CeY zeolite nanocomposites (P3MT/CeY) were prepared by chemical oxidative polymerization using anhydrous $FeCl_3$ as the oxidizing agent. The physical and chemical properties of the prepared samples were measured by various characterization techniques, such as conductivity measurement, Fourier-transform infrared spectroscopy (FT-IR), scanning electron microscopy (SEM), X-ray diffraction (XRD), thermogravimetric analysis (TGA) and carbon-sulfur analysis. The prepared P3MT/CeY composites retained the crystalline structure of Y zeolite, which also enhanced thermostability. A 2000-fold increase in conductivity relative to a blank prepared using P3MT was observed for the composite prepared using a 3:1 g/mL ratio of CeY and P3MT.

1 Introduction

Conducting polymers have shown tremendous prospect for their applications in the fields of electronics[1], energy[2] and biology[3]. Polythiophene and its derivatives are of particular interest due to their ease of synthesis and high environmental stability and have been actively researched for more than two decades[4, 5]. When the conductivity of polythiophene is higher than 10^{-6} S/cm, it will has the potential to be used as a semi conductive polymer, and can be used in light emitting diodes, field-effect transistors, photodetectors, photovoltaic cells,

*Corresponding author: Weiren Bao, Tel.: +86 351 6010482; fax: +86 351 6010482.
E-mail: baoweiren@tyut.edu.cn

optocouplers and light modulators[6]. Guo *et al*.[7] synthesized a LiV_3O_8/polythiophene composite, and found that the composite with high electronic conductivity (~10^{-3} S/cm) and good cycling performance, which could be used as a promising cathode material for lithium ion batteries. Poly(3-hexylthiophene) with high carrier density and conductivity was achieved by electrostatic charge injection, and thus its field-effect mobility was improved dramatically compared with oligomeric semiconductors [8]. Tong *el al*[9] reported an Au/polythiophene/Au device with a sandwich structure, which has high conductivity (~10 S/cm) and exhibit strong photoresponses. One such derivative, Poly(3-methylthiophene) (P3MT), is of importance due to its application in a variety of devices, such as sensors, super capacitors, light-emitting devices and photovoltaic cells.

Many studies[10, 11] have attempted to develop hybrid P3MT-inorganic nanocomposites. The addition of inorganic material can not only improve composite stability, but also enhance their performance in other applications. Hybrid nanocomposites composed of P3MT and Gold, Platinum, Palladium or Copper metal nanoparticles have been shown to exhibit excellent electrocatalytic activity towards the oxidation of iodate[12], dopamine[13, 14], uric acid[14], acetaminophen[15], nitrite[12, 16], methanol[16], ascorbic acid[13-15] and glucose[17]. Bhattacharya et al.[18] synthesized a P3MT/graphene composite via chemical oxidative polymerization and reported its use as a supercapacitor with specific capacitance of 240 F/g. Lagoutte *et al*.[19] reported that the nanocomposites synthesized by the electrodeposition of P3MT onto long, thick and vertically aligned carbon nanotubes exhibited a large capacitance of 126 F/g. P3MT composites also presented excellent photoluminescence properties. When Cu was coated onto the P3MT film by a sequential electrochemical method in an anodic alumina oxide

nanoporous template, the PL peak intensity for the hybrid P3MT/Cu film showed a 100-fold enhancement when compared to that of the P3MT single nanotube[20]. After the gold nanoparticles were fabricated on the surface of the P3MT nanotubes, the emission spectrum of P3MT dramatically changed from green to bright red, and the PL peak intensity for the increased by ~200 times relative to that of P3MT nanotube[21]. Wang *et al.*[22] prepared stable P3MT/WO_3 nanocomposite films with high electrochemical activity and stability, whilst Lin *et al.*[23] prepared organic-inorganic hybrid material based on P3MT and TiO_2. The photovoltaic cell fabricated from P3MT/TiO_2 donor/acceptor hybrid showed good photoelectric performance. Sydorov *et al.*[24] produced ZnO and P3MT composites which exhibited photovoltaic activity due to their hybrid organic–inorganic heterostructure. Mokhtari *et al.*[25] prepared P3MT-coated polyester fabric by a chemical polymerization process, which demonstrated electrochromic and piezochromic behaviors.

Y zeolite demonstrates remarkable stability and is commonly used as a commercial adsorbent and catalyst. Previous work shows that it is possible to ion-exchange the metal ion into the zeolite channel, leading to an improvement in conductivity. Additionally, it is possible to enhance the stabilization of P3MT by forming a composite with Y zeolite[26]. From our previous studies, CeY zeolite(CeY) demonstrate excellent adsorption of thiophene and its derivatives from crude benzene solution when compared with ZSM-5, silica gel and γ-Al_2O_3[27-31]. The main focus of this work is to recycle the used CeY, along with thiophene and any of its derivatives extracted from crude benzene. In this study, a series of P3MT/CeY samples were prepared by chemical oxidative polymerization using $FeCl_3$ as oxidant so as to investigate their properties, which to the best of our knowledge, have not yet been determined.

The composition, morphologies, structural features and thermal stabilities of the P3MT/CeY composites were analyzed using carbon-sulfur analysis, scanning electron microscopy (SEM), X-ray diffraction (XRD), FT-IR spectroscopy and thermogravimetric analysis (TGA). The conductivities of prepared samples were measured and correlated to the observed structures.

2 Experimental

2.1 Preparation of samples

CeY with excellent adsorption capabilities towards thiophene present in crude benzene was prepared from commercial NaY zeolite by the following method. The commercial NaY zeolite, having Si/Al ratio of 5:1, was ion-exchanged in $Ce(NO_3)_3$ solution (0.1 mol/L) at 100 ^oC in a heating reflux apparatus, using 10 mL $Ce(NO_3)_3$ solution per 1 g NaY zeolite. The sample was washed thoroughly with deionized water, oven-dried at 120 ^oC for 10 h, and then calcined at 700 ^oC for 2 h. The above steps were repeated to increase the amount of ion-exchanged Ce in the zeolite.

P3MT was prepared in a 250 mL conical flask. Firstly, 10 g of $FeCl_3$ were dispersed in 25 mL $CHCl_3$ by 30 minutes of ultrasonication. 1.45 mL of 3-methylthiophene monomer (3MT) was added to the P3MT whilst maintaining the reaction temperature at 0 ^oC, after which the reaction mixture was magnetically stirred for 12 h. The product was then filtered and then dried in a vacuum oven at 50 ^oC for 24 h. The P3MT/CeY composites were synthesized using the same approach, with the CeY zeolite being added prior to addition of 3MT. Samples having different ratios of CeY zeolite mass (m_{CeY}, g) to 3MT volume (V_{3MT}, mL) were prepared as listed in **Table 1**, in which *r* in PMTY*r* denotes the CeY zeolite dosage per 10 mL 3MT used during the preparation of the P3MT/CeY composites. PMTYB is the

blank sample prepared via the same process except for the addition of 3MT.

Table 1 Codes of samples prepared in different conditions

m_{CeY} : V_{3MT} (g/mL)	2.0	2.5	3.0	3.5	4.0	-
Codes of samples	PMTY20	PMTY25	PMTY30	PMTY35	PMTY40	PMTYB

2.2 Characterization of samples

Crystallographic analysis of the sample was performed using a D/max-2500 model X-ray diffractometer (Rigaku, Japan) with Cu-Kα radiation source (λ=0.154 nm), 40 kV tube voltage and 100 mA tube current. Thermal stability measurements were carried out on a STA409C Thermogravimetric Analyser (Netzsch, Germany) in air with a flow rate of 80 mL/min and a heating rate of 10 K/min. Surface morphology characterization was performed using a JSM-6700F Scanning Electron Microscope (JEOL Ltd., Japan) with an accelerating voltage of 10 kV.

FT-IR spectra of the sample were obtained on a Bruker VERTEX 70 model instrument (Bruker, Germany) in absorbance mode at room temperature, with a repetition of 16 scans at 4 cm^{-1} resolution. For FT-IR analysis, 1 mg of sample and 100 mg KBr were finely ground together and then pressed into a translucent pellet. Figure 1(a) shows the typical FT-IR spectrum of the P3MT/CeY composite. the peak at 1447 cm^{-1} is attributed to symmetric C=C stretching vibrations of the 3MT ring[32], and the peak observed at 797 cm^{-1} is the characteristic peak of C_α-$C_{\alpha'}$ bonds between 3MT rings in the polymer[33]. Because the C=C bonds can exist in several poly(3-methylthiophene) with different C-C connection forms, if we divide the area of the peak at 797 cm^{-1} by that of the peak at 1447 cm^{-1} as list in equation (1), the R_A can be used to describe the relative content of the poly(3-methylthiophene) with C_α-C_α connection

modes.

$$R_A = \frac{A_{C\alpha-C\alpha'}}{A_{\upsilon=1442}} \quad (1)$$

where $A_{C\alpha\text{-}C\alpha'}$ and $A_{\upsilon=1442}$ are the area of the peak around 797 cm^{-1} and 1447 cm^{-1} in FT-IR spectrum of samples, respectively.

In order to calculate R_A, the bands around 797 cm^{-1} and 1447 cm^{-1} were deconvoluted as show in Figure 1(b) and Figure 1(c) respectively. The bands around 708 cm^{-1} and 821 cm^{-1} belong to out-of-plane C-H deformation of α and β position of 3MT, respectively[21]. The weak peak around 740 cm^{-1} can be attributed to the $\delta(C_\beta\text{-H})$ vibration band[33], and the peaks at 1392 cm^{-1} corresponds to deformation of methyl groups in P3MT[21, 31].

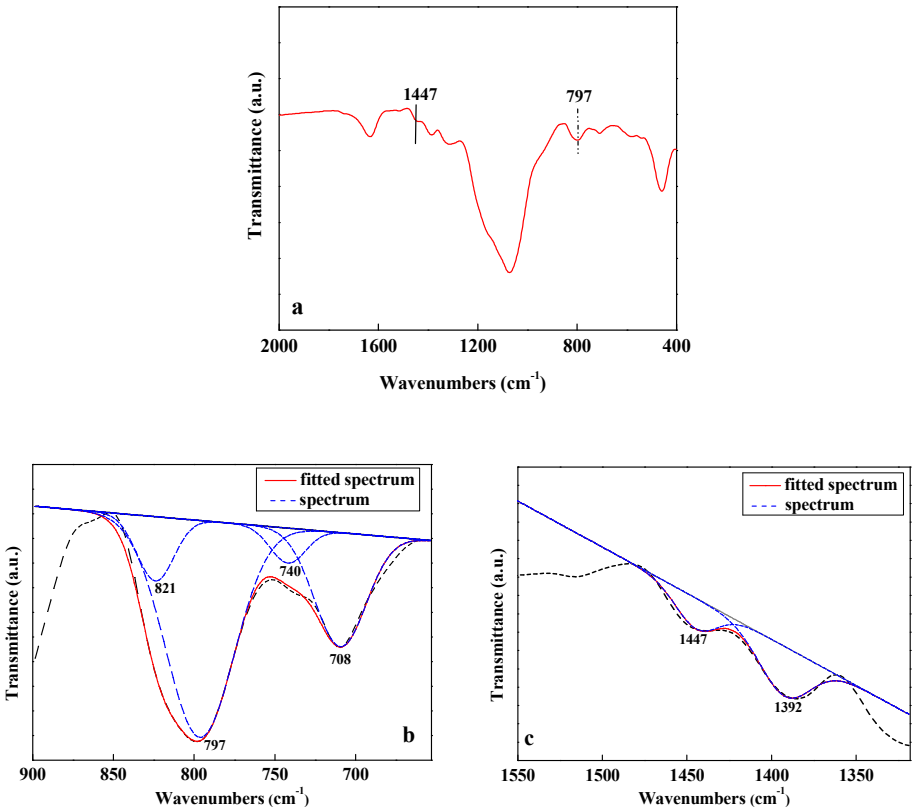

Fig. 1 A typical FTIR spectrum of the composite (a) and the deconvolution of brands around 653~890 cm^{-1}(b) and 1318~1550 cm^{-1}(c)

Sample conductivity was studied using a ZC-36 ohmmeter (Shanghai Qiangjia Electrc Co., Ltd., China). P3MT and the composite materials were ground and then characterized on pressed wafers. Wafer thickness and diameter were measured using a vernier caliper.

Carbon and sulfur content of sample were measured by a HCS-140 infrared carbon-sulfur analyzer (Shanghai Dekai Instrument Co., Ltd., China). The theoretical sulfur content of CeY/P3MT composite based on CeY zeolite ($S_{\text{Theoretical}}$) was calculated on the basis of the assumption that all the added 3MT successfully polymerized to form the P3MT present in the resulting CeY/P3MT composite, as shown in equation (2). The conversion of 3MT (X_{3MT}) can be calculated using equation (3).

$$S_{\text{Theoretical}} = \frac{\rho_{3MT} M_{sulfur}}{M_{3MT}} \times \frac{1}{m_{CeY}/V_{3MT}} \times 100\% \quad (2)$$

$$X_{3MT} = \frac{S_{\text{Measured}}}{S_{\text{Theoretical}}} \times 100\% \quad (3)$$

where ρ_{3MT} is the density of 3MT (g/mL), M_{sulfur} and M_{3MT} are the relative molecular mass of sulfur and 3MT, respectively, and S_{Measured} is the sulfur content measured in the CeY/P3MT samples based on CeY zeolite using infrared carbon-sulfur analysis.

3 Results and discussion

3.1 Conductivity of samples

The measured results of conductivity of different samples are shown in **Table 2**. The conductivity of PMTYB is very low, whereas that of other P3MT/CeY samples is much higher. The ratio of CeY zeolite mass and 3MT volume obviously influences the electrical properties of the composites, with PMTY30 having the highest conductivity, with a value of 3.2×10^{-6} S/cm, which is about two thousand times higher than that of PMTYB. There are two probable reasons for the increase in conductivity of samples. Firstly, cerium in CeY zeolite is

a metal ion which in itself is a good electrical conductor, leading to an increase in the conductivity for P3MT/CeY. Secondly, in the P3MT/CeY nanocomposite, the Ce-S bond could be formed by movement of the 3MT lone-pair electrons to the empty orbitals of the cerium ion; the resulting reduction in electron density around the 3MT would yield a more stable composite, which in turn could improve the conductivity.

Table 2 Conductivities of samples

Samples	PMTY20	PMTY25	PMTY30	PMTY35	PMTY40	PMTYB
Conductivity ($\times 10^{-8}$ S/cm)	8	21	320	110	66	0.13

3.2 Composition and structure characteristics of samples

In order to verify the existence of P3MT, the prepared samples were characterized by FT-IR spectroscopy, as shown in **Fig. 2**. It can be seen that the P3MT sample prepared without CeY presents a number of characteristic peaks. The peaks at 1636 cm^{-1} and 1447 cm^{-1} pertain to C–C stretching vibrations and C=C stretching vibration of the thiophene ring[21], respectively. The peaks at 1383 cm^{-1} and 1298 cm^{-1} correspond to deformation of methyl groups in P3MT[21, 31]. The bands around 708 cm^{-1} and 821 cm^{-1} belong to out-of-plane C-H deformation of α and β position of 3MT, respectively[21]. The peak at 856 cm^{-1} corresponds to the C-S bond in P3MT polymer[21,31]. The FT-IR spectra of P3MT/CeY composites present very different peak results to those discussed previously. The peaks at 1066 cm^{-1} and 460 cm^{-1} of the blank sample (PMTYB) are assigned to Si-O stretching vibrations and bending vibrations of CeY zeolite, respectively[34], whereas the peaks at 805 cm^{-1} and 575 cm^{-1} are indicative of Si-O-Si vibrations of CeY[35]. Compared with PMTYB, new peaks appear in FT-IR spectra of P3MT/CeY at 1392 cm^{-1}, 1319 cm^{-1}, 797 cm^{-1} and 699 cm^{-1}, which are shifted relative to the

peaks in the P3MT FT-IR spectrum, with values of 1383 cm^{-1}, 1298 cm^{-1}, 821cm^{-1} and 708 cm^{-1}. This shift is probably due to the chemical interaction between P3MT and CeY zeolite. Formation of the S-Ce bond by Ce^{3+} in CeY and S from 3MT, leads to an increase in conjugation of the P3MT, which results in the enhancement of the electron withdrawing effect of the π-bond to C_α-H and C_β-H in 3MT, which in turn leads to shifting of the peaks to the lower wavenumbers of 708 cm^{-1} and 821 cm^{-1}, respectively. On the contrary, increased conjugation weakens the methyl-thiophene ring bonds, and the IR peaks of 1383 cm^{-1} and 1298 cm^{-1} move to higher wavenumbers. In the prepared P3MT/CeY samples, the extent of peak shift did not change on varying the ratio of CeY mass and 3MT volume during synthesis of the composite, although peak intensity was different.

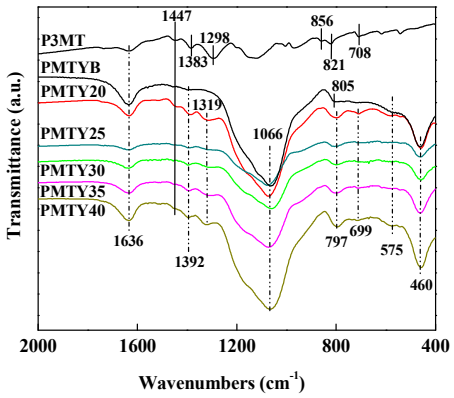

Fig. 2 FT-IR spectra of P3MT and P3MT/CeY composites

In order to explain the difference in electrical conductivity, it is necessary to understand the physical and chemical properties of the prepared samples. It can be observed from **Fig. 3** that R_A values of P3MT/CeY samples show a linear relationship with the nature logarithm of their conductivities, which should explain the conductivity results from **Table 3**. It can be concluded that the PMTY30 sample shows the highest conductivity and C_α-$C_{\alpha'}$ connection

content from the prepared P3MT samples, and hence should be further analyzed in terms of crystalline structure, surface morphology and thermal stability.

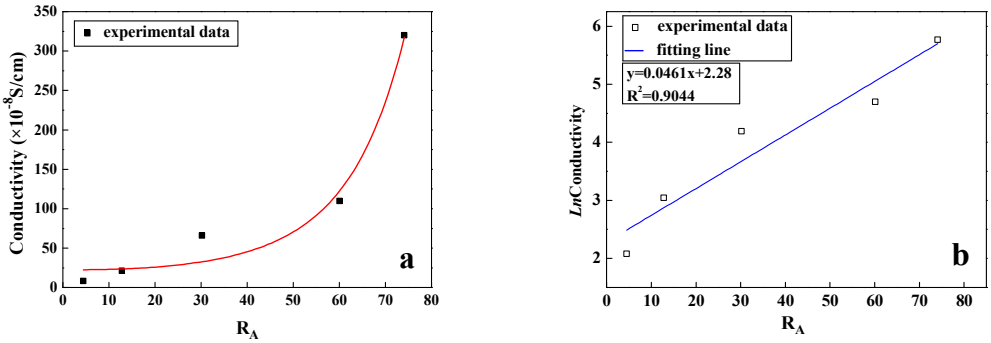

Fig. 3 Effect of relative peak area of C_{α}-$C_{\alpha'}$ in P3MT on conductivity of P3MT/CeY (a) and the fitting results (b)

Fig. 4 displays the SEM and EDS images of P3MT, PMTYB and PMTY30. As shown in **Fig. 4(a)**, P3MT has a smooth surface appearance and uniform color, while for PMTYB, lots of particles could be observed (**Fig. 4(b)**). From **Fig. 4(c)**, it can be seen that the surface of PMTY30 is similar to that of PMTYB, indicating that the P3MT polymer does not alter the surface morphology of CeY zeolite after formation of the composite. From the EDS results of these three samples, it can be seen that P3MT mainly contains carbon and sulfur from the 3MT monomer, and also contains iron and chlorine which are from the anhydrous $FeCl_3$ used as an oxidizing agent in the reaction. Moreover, PMTYB and PMTY30 all consist primarily of Si, Al, O and Ce which are all present within CeY zeolites. The presence of C and S in PMTY30 also indicates that P3MT was composited with CeY zeolite.

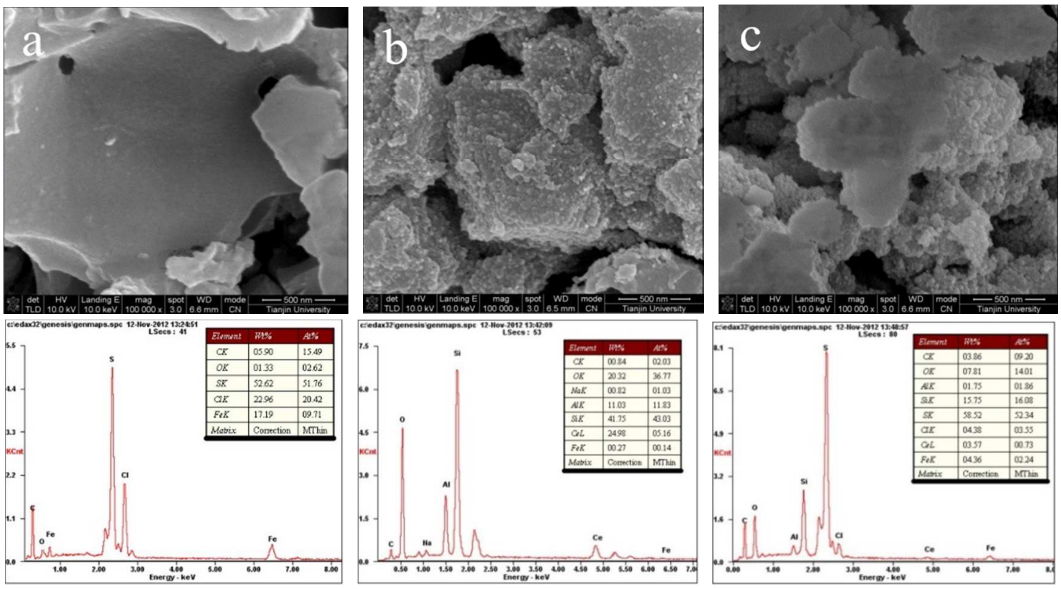

Fig. 4 SEM and EDS images of P3MT (a), PMTYB (b) and PMTY30 (c)

Fig. 5 shows XRD patterns of P3MT, PMTYB and PMTY30. Obviously, the structure of P3MT is non-crystalline, which is consistent with literature[25]. The positions of the peaks in both PMTYB and PMTY30 samples are very similar to each other, indicating that P3MT/CeY composites still can retain the crystal structure of zeolite.

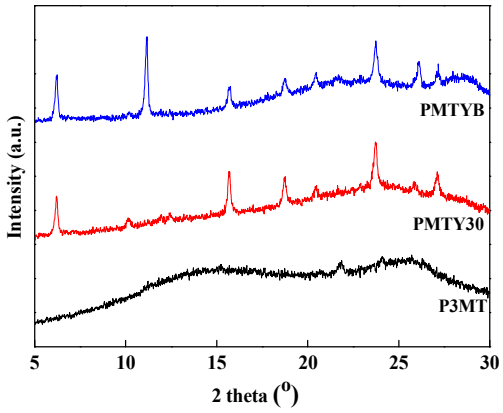

Fig. 5 XRD spectra of P3MT, PMTYB and PMTY30 samples

C-S analysis results, theoretical sulfur contents, and 3MT conversion of samples are illustrated in **Table 3**. The C and S contents both decrease with increasing CeY mass and 3MT volume ratio, which is understandable due to carbon and sulfur only being provided by the

3MT. The relationship between actual measured (*y%*) and corresponding theoretical (*x%*) values of sulfur content based on CeY zeolite in samples is shown in **Fig. 6**, which is used to describe the 3MT utilization during preparation. It can be seen that sulfur content *y* (%) and *x* (%) exhibit a linear relationship to which an equation can be fit, having formula *y=1.09x-4.76* with R^2=0.9859. Theoretically, in this equation, the intercept should be zero, but instead is -4.76. This could be due to the loss of 3MT during synthesis, since it is a volatile substance. This indicates that this preparation method has the advantage of less 3MT loss (4.76%).

Table 3 C and S contents, theoretical sulfur contents, and % conversion of 3MT of prepared samples

Samples	Carbon content (wt %)	$S_{Measured}$ (wt %)	$S_{Theoretical}$ (wt %)	X_{3MT} (%)
PMTY20	30.2	13.6	16.6	81.9
PMTY25	19.2	9.2	13.3	69.2
PMTY30	13.9	6.9	11.0	62.7
PMTY35	12.0	5.7	9.5	60.0
PMTY40	9.6	4.5	8.3	54.2

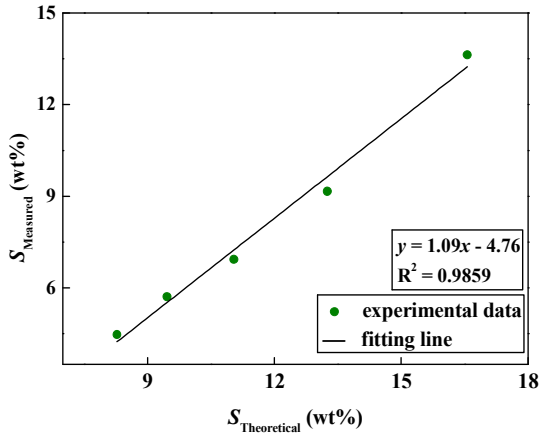

Fig. 6 Relationship between observed and corresponding theoretical sulfur content within the samples

3.3 Thermal stability of samples

TGA/DTG results of P3MT, PMTYB and PMTY30 are shown in **Fig. 7**. It can be seen that there are two weight loss steps in the TGA curves of P3MT, PMTYB and PMTY30 samples. The temperature of the first weight loss step below 200 °C can be attributed to the loss of water and organic solvent adsorbed by the zeolite, and the temperature of the other step is higher than 300 °C, which could be due to combustion of the polymer. The ignition temperature, maximum combustion temperature, burn-out temperature and burnable content of the second weight loss step are illustrated in **Table 4**. Both of these temperatures are higher for PMTY30 when compared to those of P3MT, and almost all of the P3MT decomposes before 400 °C, whereas only approximately 30 percent of P3MT in PMTY30 decomposes at the same temperature. This suggests that the thermal stability of the composites could be enhanced by CeY zeolite. Moreover, the burnable content, which represents the polymer content, are 11% and 85% for PMTY30 and P3MT, respectively. This indicates that after combustion, P3MT still retains approximately 15% of its starting mass, which can probably be attributed to the presence of $FeCl_3$, the existence of which was evinced by the EDS result of P3MT, as shown in **Fig. 4(a)**.

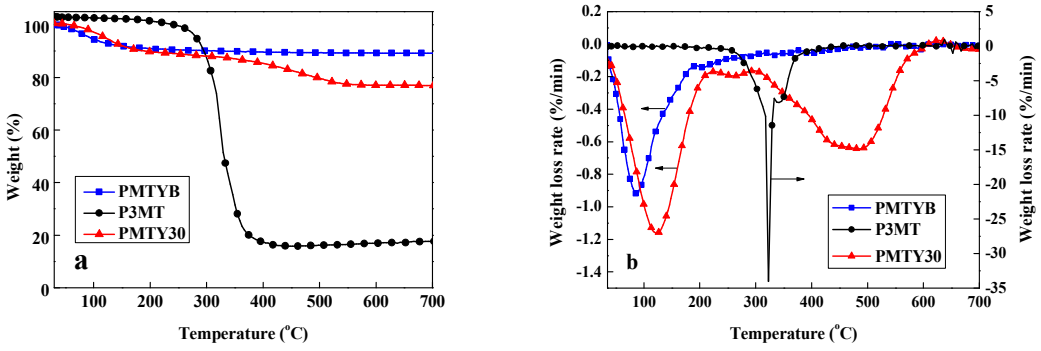

Fig. 7 TGA (a) and DTG (b) curves of P3MT, PMTYB and PMTY30 samples

Table 4 Thermal analysis results of samples

Samples	Ignition temperature (°C)	Maximum combustion Temperature (°C)	Burn-out temperature (°C)	Burnable content (%)
P3MT	220	323	430	85
PMTY30	290	480	625	11

4 Conclusions

P3MT/CeY composites were successfully synthesized by chemical oxidative polymerization of 3MT and CeY zeolite in $CHCl_3$ using anhydrous $FeCl_3$ as oxidant. P3MT exists in a non-crystalline structure, whereas the poly(3-methylthiophene)/CeY composites retain the crystal structure of Y zeolite. The conductivity of P3MT/CeY composite is higher than that of PMTYB and up to 3.2×10^{-6} S/cm. In comparison to P3MT, the thermostability of P3MT/CeY composite is greatly improved by zeolite.

Acknowledgements

The authors gratefully acknowledge the financial support of National Natural Science Foundation of China (51372161, 21406151), Research Fund for Doctoral Program of High Education (20131402110010) and Shanxi Scholarship Council of China (2012-0039).

References

1. D. Venkateshvaran, M. Nikolka, A. Sadhanala, V. Lemaur, M. Zelazny, M. Kepa, M. Hurhangee, A. J. Kronemeijer, V. Pecunia, I. Nasrallah, I. Romanov, K. Broch, I. McCulloch, D. Emin, Y. Olivier, J. Cornil, D. Beljonne and H. Sirringhaus, *Nature*, 2014, **515**, 384-388.
2. M. J. Sailor, E. J. Ginsburg, C. B. Gorman, A. Kumar, R. H. Grubbs and N. S. Lewis, *Science*, 1990, **249**, 1146-1149.
3. P. Sista, K. Ghosh, J. S. Martinez and a. R. C. Rocha, *Journal of Nanoscience and Nanotechnology*, 2014, **14**, 250-272.
4. K. Jen, G. G. Miller and R. L. Elsenbaumer, *Journal of the Chemical Society, Chemical Communications*, 1986, **17**, 1346-1347.
5. J. Ruiz, B. Gonzalo, J. M. Laza, L. M. Leon, M. I. Moreno, J. L. Vilas and E. Bilbao, *Advances in Polymer Technology*, 2014, **33**, 7.

6. R. D. McCullough, in *Handbook of Oligo- and Polythiophenes*, ed. D. Fichou, WILEY-VCH N Y, 1999.
7. H. Guo, L. Liu, H. Shu, X. Yang, Z. Yang, M. Zhou, J. Tan, Z. Yan, H. Hu and X. Wang, *Journal of Power Sources*, 2014, **247**, 117-126.
8. M. J. Panzer and C. D. Frisbie, *Advanced Functional Materials*, 2006, **16**, 1051-1056.
9. L. Tong, C. Li, F. e. Chen, H. Bai, L. Zhao and G. Shi, *The Journal of Physical Chemistry C*, 2009, **113**, 7411-7415.
10. N. Lingapppan, J. H. Jeong, J. M. Park and K. T. Lim, *Journal of Nanoscience and Nanotechnology*, 2014, **14**, 5708-5712.
11. H. Dolas and A. S. Sarac, *Synthetic Metals*, 2014, **195**, 44-53.
12. X. Huang, Y. Li, Y. Chen and L. Wang, *Sensors and Actuators B: Chemical*, 2008, **134**, 780-786.
13. N. F. Atta and M. F. El-Kady, *Sensors and Actuators B: Chemical*, 2010, **145**, 299-310.
14. X. Huang, Y. Li, P. Wang and L. Wang, *Analytical sciences*, 2008, **24**, 1563-1568.
15. N. F. Atta and M. F. El-Kady, *Talanta*, 2009, **79**, 639-647.
16. Y. Zhou, H. Xian, F. Li, S. Wu, Q. Lu, Y. Li and L. Wang, *Electrochimica Acta*, 2010, **55**, 5905-5910.
17. C. Malitesta, M. R. Guascito, E. Mazzotta, T. Siciliano and A. Tepore, *Sensors and Actuators B: Chemical*, 2013, **184**, 70-77.
18. P. Bhattacharya and C. K. Das, *Journal of Nanoscience and Nanotechnology*, 2012, **12**, 7173-7180.
19. S. Lagoutte, P. Aubert, M. Pinault, F. Tran-Van, M. Mayne-L'Hermite and C. Chevrot, *Electrochimica Acta*, 2014, **130**, 754-765.
20. D. H. Park, M.-Y. Jeong, M. Kim, E. H. Cho, D.-C. Kim, H. Song, J. Kim, T. K. Shim, D. Kim and J. Joo, *Journal of Nanoscience and Nanotechnology*, 2009, **9**, 3112-3118.
21. D. H. Park, Y. K. Hong, M. S. Kim, E. H. Cho, W. J. Choi, K. H. Kim, Q. H. Park, D.-C. Kim, H. Song, J. Kim and J. Joo, *Synthetic Metals*, 2010, **160**, 604-608.
22. X. Wang, X. C. Song, Y. F. Zheng, R. Ma and H. Y. Yin, *Journal of Experimental Nanoscience*, 2013, **8**, 546-554.
23. Y.-J. Lin, L. Wang and W.-Y. Chiu, *Thin Solid Films*, 2006, **511-512**, 199-202.
24. D. Sydorov, P. Smertenko, Y. Piryatinski, T. Yoshida and A. Pud, *Electrochimica Acta*, 2012, **81**, 83-89.
25. J. Mokhtari and M. Nouri, *Fibers and Polymers*, 2012, **13**, 139-144.
26. M. Jaymand, *RSC Advances*, 2014, **4**, 33935-33954.
27. J. Liao, L. Bao, W. Wang, Y. Xie, J. Chang, W. Bao and L. Chang, *Fuel Processing Technology*, 2014, **117**, 38-43.
28. J. Liao, W. Bao, Y. Chen, Y. Zhang and L. Chang, *Energy Sources, Part A: Recovery, Utilization, and Environmental Effects*, 2012, **34**, 618-625.
29. J. Liao, W. Wang, H. Wang, Q. Jin and L. Chang, *Modern Chemical Industry*, 2009, **29**, 219-221.
30. J. Liao, W. Wang, Y. Xie, Y. Zhang, L. Chang and W. Bao, *Separation Science and Technology*, 2012, **47**, 1880-1885.
31. J. Liao, Y. Zhang, W. Wang, Y. Xie and L. Chang, *Adsorption*, 2012, **18**, 181-187.
32. M. Akimoto, Y. Furukawa, H. Takeuchi, I. Harada, Y. Soma and M. Soma, *Synthetic Metals*, 1986, **15**, 353-360.
33. T. Yamamoto, K. Sanechika and A. Yamamoto, *Bulletin of the Chemical Society of Japan*, 1983, **56**, 1497-1502.
34. G. Bidan, O. Jarjayes, J. M. Fruchart and E. Hannecart, *Advanced Materials*, 1994, **6**, 152-155.
35. L. Lin, Y. Zhang, H. Zhang and F. Lu, *Journal of colloid and interface science*, 2011, **360**, 753-759.